Circulant determinant-based Permutation Entropy for sEMG signal processing

* M. JABLOUN, † A. HOLOBAR, † N. MURKS, † M. KRAMBERGER, * Ph. RAVIER, * O. BUTTELLI
*Orleans University - PRISME Lab, Orleans, France, meryem.jabloun@univ-orleans.fr.
† Maribor University - FEECS- SSL, Maribor, Slovenia, ales.holobar@um.si.

***Abstract*—Several approaches have been proposed to extend the permutation entropy (PE) by incorporating amplitude information, which is typically discarded in the original PE formulation. In this paper, we introduce a new PE variant that explicitly accounts for amplitude information using the well-established spectral properties of circulant determinants. This circulant determinant-based PE (CDPE) effectively captures the theoretical PE of sinusoids within the normalized frequency range $[0.01, 0.2]$, outperforming existing amplitude-dependent PE (ADPE) methods. Since this range aligns with the spectral characteristics of surface electromyography (sEMG) signals (5–500 Hz) sampled at 2048 Hz, the second key contribution of our work is investigating the sensitivity of CDPE and existing ADPE measures to excitation levels. To this end, these ADPE methods were applied to simulated physiological high-density sEMG (HDsEMG). HDsEMG represent a spatially distributed acquisition of sEMG using a dense array of electrodes, enabling a refined analysis of muscle electrical activity. Our findings provide a deeper understanding of the applicability and robustness of ADPE-based methods for HDsEMG signal analysis.**

***Index Terms*—Amplitude-dependent Permutation entropy PE, Ordinal patterns, Circulant determinant, High density surface electromyogram HDsEMG.**

I. Introduction

Surface electromyography (sEMG) represents the electrical activity of muscles recorded on the surface of the skin. sEMG signals exhibit stochastic and deterministic characteristics, influenced by the recruitment of motor units (MUs), where each MU consists of a motoneuron and its associated muscle fibers [1]. Since MU recruitment is related to force regulation and fatigue dynamics, sEMG signals are widely used as a non-invasive technique to assess these aspects of the human neuromuscular system [2].

Among the methods used in sEMG signal analysis, permutation entropy (PE) and its various extensions have emerged as promising complexity measures [3]. PE performs a threshold-free transformation of weakly nonstationary signals by ranking successive samples in ascending order, efficiently encoding them into sequences of ordinal patterns (OPs) [4]. The occurrence frequency of OPs serves as an estimate of their probability distribution, enabling computation of the Shannon entropy. Since PE relies solely on OPs and ignores amplitude information, several amplitude-dependent PE (ADPE) extensions, such as weighted PE (WPE)[5], [6], [7], [8], [9], amplitude-aware PE (AAPE) [10], [11], and dispersion entropy (DispEn) [12], [13], have been proposed to incorporate amplitude information. The WPE assigns weights to the occurrence frequency of each OP based on the variance of its corresponding sample values. In contrast, the AAPE introduces a tuning parameter to adjust the emphasis on mean amplitude values and amplitude differences. The DispEn first maps the signal data into a set of discrete classes using a predefined probability distribution before applying OP analysis.

In the present paper, we propose a new PE variant that effectively captures both OP and amplitude variations by incorporating circulant determinants into the computation of a weighted PE. This approach yields a more generalized, robust, and parameter-free PE while offering a spectral energy-based interpretation of the resulting complexity measure. The second focus of our study is to evaluate the applicability and robustness of the proposed CDPE along with existing ADPE measures for the analysis of sEMG signals. Specifically, we investigate the sensitivity of ADPE to excitation levels by analysing high-density sEMG (HDsEMG) signals, which offer a spatially detailed representation of muscle activity, allowing for improved interpretation.

The paper is organized as follows. Section II reviews the concept of PE and existing ADPE measures. Section III presents the circulant determinant-based PE (CDPE). In Section IV, a comparative study of these ADPE variants is conducted using simulated physiological HDsEMG signals. Finally, Section V concludes the paper and outlines future research directions.

II. PE and Existing Amplitude-dependent PEs

This section briefly revisits the PE and existing variants that incorporate amplitude information.

A. Permutation Entropy

A threshold-free symbolic representation of a weakly stationary and uniformly sampled time series x_t for $t = 0, 1, \ldots, N-1$ can be achieved by ranking the values within each set of d consecutive samples, $x_t, x_{t+1}, \ldots, x_{t+d-1}$. The permutation of the set $\{0, 1, 2, \ldots, d-1\}$ that sorts these sample values in ascending order is called an ordinal pattern (OP). For example, there are two possible OPs for d=2:

This research was co-funded by the Slovenian Research and Innovation Agency: **project BI-FR/25-26-PROTEUS-002 and programme P2-0041** and by the European Union's Horizon Europe Research and Innovation Program **HybridNeuro project, GA No. 101079392**. Views and opinions expressed are however those of the author(s) only and do not necessarily reflect those of the European Union or Research Executive Agency. Neither the European Union nor the granting authority can be held responsible for them.

Π_1='01' if $x_t < x_{t+1}$, and Π_2='10' otherwise. The occurrence frequency of each OP Π can be estimated as:

$$p_\Pi = \frac{\{\#t \ | \{x_t, x_{t+1}, \ldots, x_{t+d-1}\} \text{ of type } \Pi\}}{N-d+1}, \quad (1)$$

where $\#$ denotes the cardinality. The normalized PE is then defined as [4]

$$H = -\big(\log(d!)\big)^{-1} \sum_i p_{\Pi_i} \log(p_{\Pi_i}), \quad (2)$$

where $d!$ represents the total number of possible OPs of length d, assuming that equal sample values are rare. Note that for uncorrelated Gaussian noise, $p_\Pi = \frac{1}{d!}$ which implies that PE in (2) equals 1. Additionally, PE (2) has two key limitations: ambiguity in handling equal values and the omission of amplitude differences.

B. Weighted PE

Unlike PE, which only considers the ordinal aspect of the data, Weighted PE (WPE) incorporates weights into the OP probability (1), allowing it to distinguish between minor amplitude fluctuations (potentially caused by noise) and significant variations [5]. Consequently, the occurrence frequency of OP (1) is modified as follows:

$$p_\Pi = \frac{\sum_{t \big| \{x_t, x_{t+1}, \ldots, x_{t+d-1}\} \text{ of type } \Pi} w_t}{\sum_{t=1}^{N-d+1} w_t}, \text{ where} \quad (3)$$

$$w_t = \frac{1}{d-1} \sum_{i=0}^{d-1} (x_{t+i} - \bar{x}_t)^2, \text{ and } \bar{x}_t = \frac{1}{d} \sum_{i=0}^{d-1} x_{t+i}. \quad (4)$$

Note that for small d, (4) adopts the unbiased variance estimator, unlike the original formulation [5].

C. Amplitude-Aware PE

AAPE differs from WPE by incorporating both absolute mean and amplitude differences into the weight calculation for OP probability. Consequently, the weight in (3) is defined as [11]:

$$w_t = A \frac{1}{d} \sum_{i=0}^{d-1} |x_{t+i}| + (1-A) \frac{1}{d-1} \sum_{i=1}^{d-1} |x_{t+i} - x_{t+i-1}|, \quad (5)$$

where $A \in [0,1]$ is a tuning parameter that balances the influence of local mean and fluctuations.

D. Dispersion Entropy

DispEn is an ADPE that begins with mapping the original time series $\{x_t\}_{t=0,1,\ldots,N-1}$ onto c classes to form a symbolic time series $\{u_t\}_{t=0,1,\ldots,N-1}$, where $u_t \in [1,c]$. This mapping can be linear, by sorting all sample values and dividing them into equal-sized classes, or nonlinear, using sigmoid functions or the normal cumulative distribution. Each subsequence $\{u_t, u_{t+1}, \ldots, u_{t+d-1}\}$ defines a dispersion pattern. The occurrence frequency of a given pattern is obtained from (1) by replacing x_t with the symbolic time series u_t. Finally, the normalized DispEn is given by

$$H = -\bigg(\log(c^d)\bigg)^{-1} \sum_i p_{\Pi_i} \log(p_{\Pi_i}), \quad (6)$$

where c^d represents the total number of possible dispersion patterns.

III. Circulant Determinant-based PE

To account for both the amplitude information and the spectral characteristics of each subsequence $\{x_t, x_{t+1}, \ldots, x_{t+d-1}\}$, we propose a new PE variant where the weights in (3) are redefined as the determinant of a circulant matrix constructed from this subsequence:

$$w_t = \big|\det(X_t)\big| \text{ where} \quad (7)$$

$$X_t = \begin{bmatrix} x_t & x_{t+1} & x_{t+2} & \cdots & x_{t+d-1} \\ x_{t+d-1} & x_t & x_{t+1} & \cdots & x_{t+d-2} \\ x_{t+d-2} & x_{t+d-1} & x_t & \cdots & x_{t+d-3} \\ \vdots & \vdots & \vdots & \ddots & \vdots \\ x_{t+1} & x_{t+2} & x_{t+3} & \cdots & x_t \end{bmatrix}. \quad (8)$$

The determinant of this circulant matrix (8) is directly related to the Discrete Fourier Transform (DFT) of its generating vector [14] and can be expressed as:

$$w_t = \prod_{k=0}^{d-1} \big|\lambda_k\big|, \quad \text{with eigenvalues} \quad \lambda_k = \sum_{i=0}^{d-1} x_{t+i} e^{-j\frac{2\pi i k}{d}}, \quad (9)$$

and $j^2 = -1$. This circulant determinant, and consequently the weight assigned to each OP using (7) in combination with (3), captures the spectral characteristics of the OP related subsequences. A well-distributed spectral content across frequencies contributes to a high circulant determinant. In contrast, structured patterns, redundancy, or periodicity in the data may lead to a quasi-zero circulant determinant.

To avoid trivial cases where $\lambda_0 = \sum_{i=0}^{d-1} x_{t+i} = 0$, one can calculate

$$w_t = \big|\det(X_t - \alpha \mathbf{1})\big| = \big|\lambda_0 - \alpha d\big| \prod_{k=1}^{d-1} \big|\lambda_k\big|, \quad (10)$$

where $\mathbf{1}$ is a $d \times d$ matrix filled with ones, and α is an offset, for example, $\alpha = \min(\{x_t\}_{t=0,1,\ldots,N-1})$. Next, three examples illustrate CDPE's performance.

A. CDPE for uncorrelated Gaussian noise

The theoretical CDPE (3) (7) of white Gaussian noise (WGN) is 1 (see Appendix A for proof with d=3). Table I presents the mean $\pm$ standard deviation (STD) of ADPE measures, averaged over 150 Monte Carlo (MC) runs with $N = 5000$ samples. For $d = 3$ to 6, PE remains closest to the theoretical value. While CDPE shows the highest STD for $d \geq 4$, it performs similarly to AAPE and ImpPE. In contrast, DispEn deteriorates for $c = d > 4$. Figure 1a further illustrates the ADPE behaviour for WGN, emphasizing the impact of the sample size N. Although all ADPE methods require sufficiently large N, AAPE and PE are the least sensitive to small sample sizes.

TABLE I: Mean ± STD of ADPE measures for WGN (N = 5000, 150 MC runs)

ADPE	$d=3$		$d=4$		$d=5$		$d=6$	
	Mean	STD	Mean	STD	Mean	STD	Mean	STD
PE	0.9998	0.0002	0.9994	0.0002	0.9976	0.0004	0.9888	0.0007
CDPE	0.9997	0.0002	0.9893	0.0023	0.9786	0.0027	0.9366	0.0056
ImpPE	0.9997	0.0002	0.9989	0.0004	0.9964	0.0005	0.9846	0.0009
AAPE	0.9993	0.0003	0.9990	0.0003	0.9973	0.0005	0.9885	0.0007
DispEn (c=3)	0.9993	0.0002	0.9983	0.0004	0.9956	0.0006	0.9370	0.0052
DispEn (c=d)	0.9993	0.0002	0.9955	0.0005	0.9553	0.0014	0.7854	0.0005

B. CDPE for Sinusoidal Signals

Figures 1b and c illustrate the ADPE performance on a noise-free sinusoid $x_t = \sin(2\pi\nu t)$, as a function of the normalized frequency ν. The sample size is $N = \lfloor 500/\nu \rfloor$. As seen in these figures, the CDPE outperforms other ADPEs for $\nu \in [0.01, 0.2]$, , accurately capturing the theoretical PE of a sinusoid: 0.3869 for d=3 and 0.2181 for d=4. This superior performance is further validated in fig. 1d–1f, where the sinusoid is embedded in white Gaussian noise (WGN) at a signal-to-noise ratio (SNR) of 12 dB. The results, averaged over 150 MC runs, confirm CDPE lower values and its greater robustness to noise for $\nu \in [0.01, 0.2]$.

Accurately capturing signal complexity in this frequency range is essential for reliable sEMG interpretation. sEMG signals span 5–500 Hz [15], corresponding to a normalized frequency range of [0.0024, 0.2441] at F_s=2048 Hz. Moreover, sEMG recordings generally exhibit moderate SNR levels.

C. CDPE for Synthetic sEMG

The ADPEs are applied 1000 MC realizations of synthetic sEMG signals generated using the model in [16]. This model simulates filtered WGN with a known power spectral density (PSD) controlled by two frequency parameters, f_l and f_h:

$$PSD(f) \propto \frac{f_h^4 f^2}{(f^2 + f_l^2)(f^2 + f_h^2)^2}. \tag{11}$$

As shown in fig. 2, CDPE consistently exhibits the lowest values among the ADPEs, even when artificial noise is added.

IV. Application to HDsEMG signals

This section introduces the HDsEMG dataset and analyzes the simulated HDsEMG signals using PE (1) (2), CDPE (2), (3), (7) and DispEn (6) (c=3 classes and a normal cumulative distribution). The goal is to examine ADPE sensitivity to excitation levels, which can provide insights into motor unit recruitment and neuromuscular activation.

A. Simulated HDsEMG Dataset

The synthetic HDsEMG signals were generated using MU action potentials (MUAPs) estimated from HDsEMG recordings of slow, fatiguing contractions of the Abductor Pollicis Brevis muscle in healthy subjects. A total of 124 MUs were identified via the Convolution Kernel Compensation (CKC) algorithm [17], and their MUAPs were estimated via spike-triggered averaging, using the identified MU discharges as triggers. For each MU, its MUAPs were assigned to one of 36 discrete fatigue levels, allowing controlled MU fatigue in synthetic HDsEMG signals. MUAPs were then combined with the MU recruitment and firing modulation model from [18].

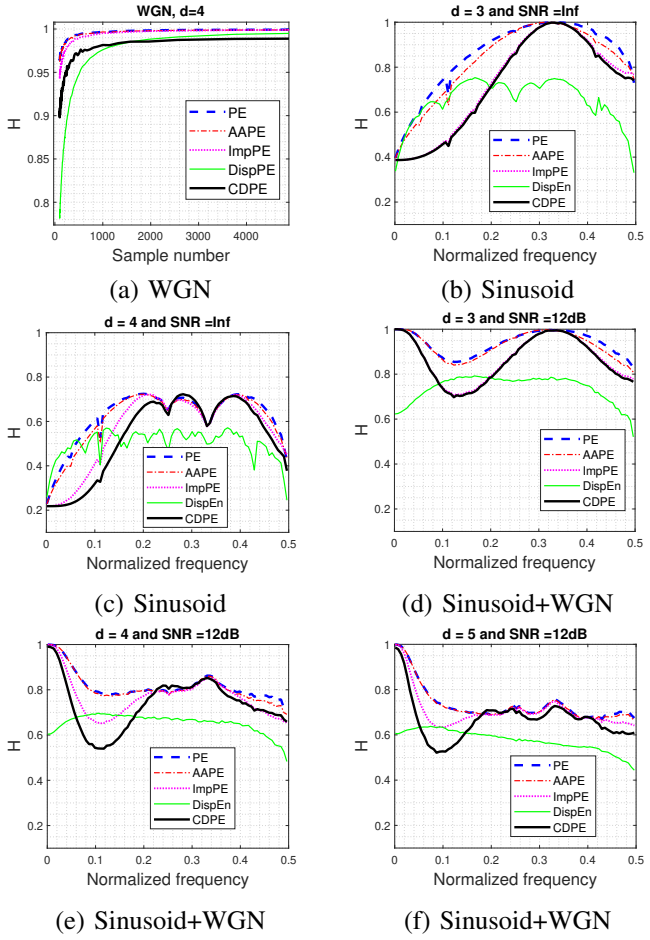

(a) WGN (b) Sinusoid (c) Sinusoid (d) Sinusoid+WGN (e) Sinusoid+WGN (f) Sinusoid+WGN

Fig. 1: Comparison of ADPEs applied to: (a) WGN with varying sample size N and d=4. (b), (c) a pure tone sinusoid with d=3 and 4, respectively. (d)-(f) pure tone sinusoid embedded in additive WGN at SNR=12 dB with d=3, 4, and 5. Results are averaged over 150 MC realizations. AAPE and DispEn are computed using A=0.5, and $c = d$, respectively.

Five recordings were analysed with a ramp excitation pattern (0% $\rightarrow$ 50% of maximum voluntary contraction (MVC)) at a constant 0% fatigue level. Each HDsEMG channel was 50 seconds long (see fig. 3a), sampled at F_s=2048 Hz, and stored in a 2D matrix corresponding to the spatial layout of a 12×5 electrode grid. Each matrix cell contained N=100×F_s samples that represent the sEMG voltage with added noise at 20 dB SNR.

B. Varying Excitation at Constant Fatigue Level

In this study, each HDsEMG signal was divided into two non-overlapping consecutive windows, denoted as: W_1 and

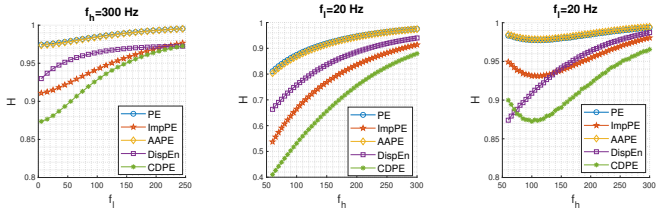

(a) (b) (c)

Fig. 2: CDPE and existing ADPEs applied to (a)-(b) simulated sEMG signal using (11). (c) Simulated sEMG embedded in an additive WGN at SNR=20 dB. F_s=2048 Hz, N=10000, d=4, A=0.5 for AAPE and $c = 3$ for DispEn.

W_2, which correspond to excitation levels of 0–30% MVC, and 30–50% MVC, respectively. The mean power spectral density (PSD) is shown in fig. 3b-c.

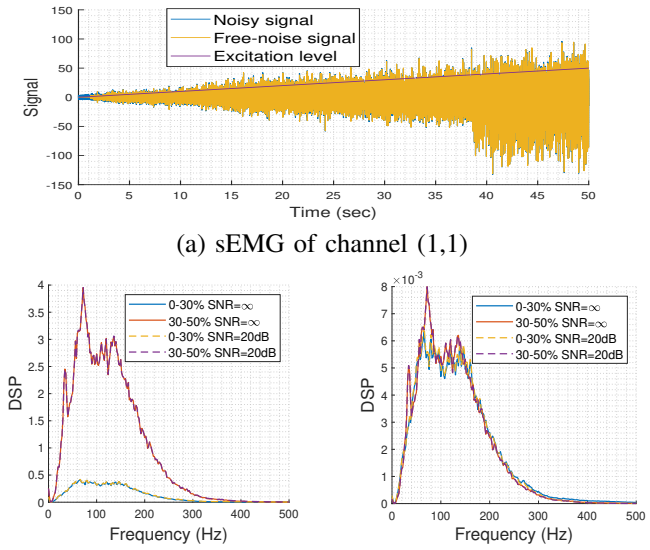

(a) sEMG of channel (1,1)

(b) Mean PSD (c) Normalized PSD

Fig. 3: Synthetic HDsEMG signals [17]: (a) Ramp excitation pattern superimposed on noisy and noise-free recordings . (b) Mean PSD and (c) normalized PSD of windows W_1 and W_2.

Table II presents the mean ADPE values averaged over the 12×5 HDsEMG matrix while fig. 4 provides a channel-wise comparison of CDPE, DispEn, and PE for d=5 at SNR ∞ and 12 dB. To quantify the relative change in complexity between consecutive windows W_1 and W_2, we use the Normalized Difference Index (NDI):

$$\Delta_{1\to 2} = \left(H_{W_2} - H_{W_1}\right)\left(H_{W_2} + H_{W_1}\right)^{-1}. \qquad (12)$$

In fig. 4, the NDI results are expressed as percentages and displayed as a 12×5 matrix, reflecting the spatial electrode grid. From fig. 4, the results obtained with DispEn at SNR ∞ appear to align closely with physiological expectations. Physiologically, as excitation increases from 0 to 30% MVC, the spatial and temporal irregularity of sEMG signals increases

TABLE II: Mean CDPE, DispEn, and PE of HDsEMG recordings at different SNR and d values for W_1 and W_2.

		SNR = 20 dB		**SNR = ∞**	
Method	**d**	W_1: 0-30%	W_2: 30-50%	W_1: 0-30%	W_2: 30-50%
CDPE	3	0.5002	0.4777	0.4743	0.4742
	4	0.3459	0.3318	0.3296	0.3288
	5	0.3123	0.3031	0.3035	0.3011
DispEn	3	0.6826	0.7175	0.6388	0.7144
	4	0.6437	0.6748	0.5942	0.6711
	5	0.6189	0.6478	0.5657	0.6437
PE	3	0.8221	0.7636	0.7397	0.7553
	4	0.7383	0.6648	0.6364	0.6532
	5	0.6964	0.6127	0.5828	0.5991

rapidly due to MU recruitment [18], [17]. For excitation levels between 30 and 50% MVC, the complexity of sEMG may continue to increase slightly as MU recruitment approaches saturation.

The NDI of DispEn values (see fig. 4.c and 4.d) for both SNR conditions show the highest values. This is because DispEn is highly sensitive to amplitude variations between W_1 and W_2, as evidenced by the PSD in fig. 2.b. In contrast, PE is less affected by amplitude variations but is highly sensitive to noise. Even moderate noise levels (e.g., 20 dB) can obscure physiological changes across HDsEMG channels, making PE less reliable in noisy conditions.

Unlike DispEn and PE, CDPE exhibits greater robustness to noise in HDsEMG signals and can differentiate electrode locations within the spatial matrix (see fig. 4.a and b). CDPE captures variations in both the frequency content of the PSD and the underlying signal structure. As shown in fig. 3.c, the emergence of a low-frequency component in W_2 may explain the observed NDI variations in certain channels. Moreover, the CDPE values reported in Table II are consistently lower than those obtained from simulated sEMG signals modelled as filtered Gaussian noise with a spectral band of 20–300 Hz (see fig. 2.b-c). This suggests the presence of an inherent structure in the recorded HDsEMG signals, distinguishing them from correlated Gaussian noise.

V. Conclusions

We introduce Circulant Determinant-based PE (CDPE), a novel permutation entropy method that incorporates amplitude information via circulant determinant spectral properties. Applied to simulated physiological HDsEMG signals under controlled excitation levels without fatigue, CDPE effectively captures complexity variations of sEMG signals across multiple locations in the matrix representing the spatial electrode locations. Unlike Dispersion Entropy (DispEn), which is more sensitive to amplitude variation than the frequency content, CDPE responds to both. These results highlight CDPE relevance to sEMG analysis, with future work exploring fatigue level effects.

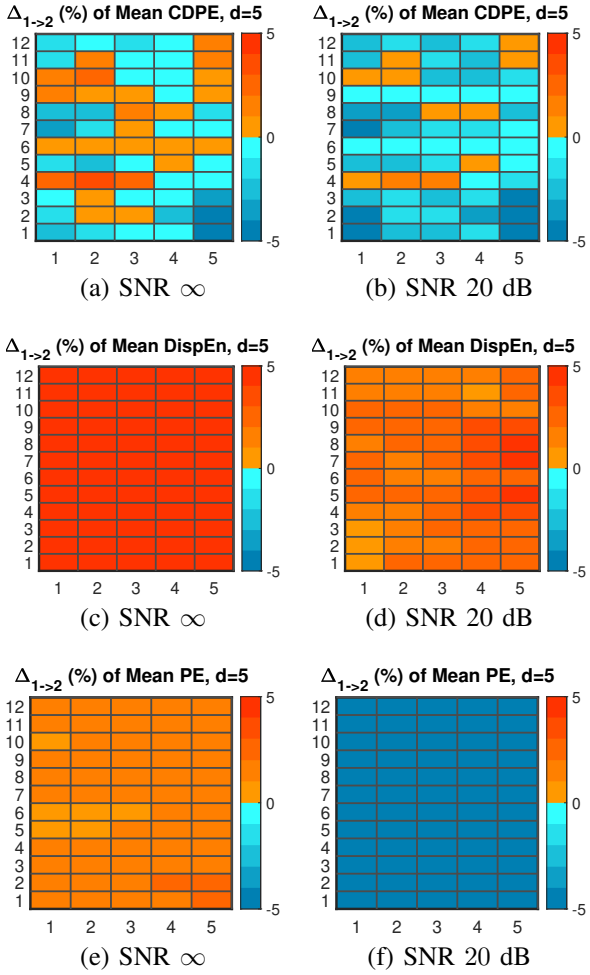

(a) SNR ∞ (b) SNR 20 dB

(c) SNR ∞ (d) SNR 20 dB

(e) SNR ∞ (f) SNR 20 dB

Fig. 4: Comparison between CDPE (top row), DispEn (middle row), and PE (bottom row) with $d = 5$, applied to HDsEMG signals. The NDI (12) is calculated using W_1 : 0–30% MVC and W_2 : 30–50% MVC for each channel acquired under varying excitation at a constant fatigue level. The NDI results are displayed as a 12×5 matrix in (%), corresponding to the spatial electrode grid. The left column represents SNR ∞, while the right column represents SNR 20 dB.

APPENDIX

Consider a centred WGN x_t with unit variance, and let $\{r_0, r_1, r_2\}$ be the sorted sequence of $\{x_t, x_{t+1}, x_{t+2}\}$. To evaluate the expected weight in (10) for $d = 3$, the determinant $\det(X_t - \alpha\mathbf{1})$ is expressed as:

$$\begin{aligned}\det(X_t - \alpha\mathbf{1}) = r_0^3 + r_1^3 + r_2^3 - 3r_0r_1r_2 \\ - 3\alpha(r_0^2 + r_1^2 + r_2^2 - r_0r_1 - r_0r_2 - r_1r_2).\end{aligned} \quad (13)$$

Given the joint probability density function of $\{r_i\}_{i=0,1,2}$:

$$f_{r_0,r_1,r_2}(u, v, w) = 3!p(u)p(v)p(w)\mathbf{1}_{(u\le v\le w)}, \quad (14)$$

where $p(u)$ is the normal pdf, the following expected values can be derived:

$$\begin{aligned} &E[r_2] = -E[r_0] = \tfrac{3}{2\sqrt{\pi}}, && E[r_1] = 0, \\ &E[r_1^2] = 1 - \tfrac{\sqrt{3}}{\pi}, && E[r_0^2] = E[r_2^2] = 1 + \tfrac{\sqrt{3}}{2\pi}, \\ &E[r_0r_2] = -\tfrac{\sqrt{3}}{\pi}, && E[r_1r_2] = E[r_0r_1] = \tfrac{\sqrt{3}}{2\pi}, \\ &E[r_1^3] = 0, && E[r_2^3] = -E[r_0^3] = \tfrac{15}{4\sqrt{\pi}}, \\ &E[r_0r_1r_2] = 0. \end{aligned} \quad (15)$$

For an appropriate α ensuring $\det(X_t - \alpha\mathbf{1}) > 0$ in (13), the expected weight related to each OP is $9|\alpha|$. This result leads to a uniform pattern distribution with occurrence frequency $p_i = \frac{1}{6}$ and a normalized CDPE $= 1$.

REFERENCES

[1] M. Dimitriou, Enhanced muscle afferent signals during motor learning in humans, Current Biology 26 (8) (2016) 1062–1068.

[2] J. S. Karlsson, K. Roeleveld, C. Grönlund, A. Holtermann, N. Östlund, Signal processing of the surface electromyogram to gain insight into neuromuscular physiology, Philos. Trans. R. Soc. A. 367 (1887) (2009) 337–356.

[3] M. Jabloun, O. Buttelli, P. Ravier, Legendre polynomial fitting-based permutation entropy offers new insights into the influence of fatigue on surface electromyography signal complexity, Entropy 26 (10) (2024).

[4] C. Bandt, B. Pompe, Permutation entropy: A natural complexity measure for time series, Phys. Rev. Lett. 88 (2002) 174102.

[5] B. Fadlallah, B. Chen, A. Keil, J. Príncipe, Weighted-permutation entropy: A complexity measure for time series incorporating amplitude information, Phys. Rev. E. 87 (2) (2013) 022911.

[6] J. Xia, P. Shang, J. Wang, W. Shi, Permutation and weighted-permutation entropy analysis for the complexity of nonlinear time series, Commun. Nonlinear Sci. Numer. Simul. 31 (1) (2016) 60–68.

[7] M. El Sayed Hussein Jomaa, P. Van Bogaert, N. Jrad, N. E. Kadish, N. Japaridze, M. Siniatchkin, M. A. Colominas, A. Humeau-Heurtier, Multivariate improved weighted multiscale permutation entropy and its application on EEG data, Biomed. Sig. Process. Control 52 (2019) 420–428.

[8] D. Stosic, D. Stosic, T. Stosic, B. Stosic, Generalized weighted permutation entropy, Chaos: An Interdisciplinary Journal of Nonlinear Science 32 (10) (2022) 103105.

[9] D. Bai, W. Yao, S. Wang, J. Wang, Multiscale weighted permutation entropy analysis of schizophrenia magnetoencephalograms, Entropy 24 (3) (2022).

[10] A. S. Gaudêncio, M. Hilal, J. M. Cardoso, A. Humeau-Heurtier, P. G. Vaz, Texture analysis using two-dimensional permutation entropy and amplitude-aware permutation entropy, Pattern Recognition Letters 159 (2022) 150–156.

[11] H. Azami, J. Escudero, Amplitude-aware permutation entropy: Illustration in spike detection and signal segmentation, Computer Methods and Programs in Biomedicine 128 (2016) 40–51.

[12] M. Rostaghi, H. Azami, Dispersion entropy: A measure for time-series analysis, IEEE Sig. Proc. Lett. 23 (5) (2016) 610–614.

[13] F. Nieto-del Amor, R. Beskhani, Y. Ye-Lin, J. Garcia-Casado, A. Diaz-Martinez, R. Monfort-Ortiz, V. J. Diago-Almela, D. Hao, G. Prats-Boluda, Assessment of dispersion and bubble entropy measures for enhancing preterm birth prediction based on electrohysterographic signals, Sensors 21 (18) (2021).

[14] R. M. Gray, Toeplitz and circulant matrices: A review, Found. Trends Commun. Inf. Theory 2 (3) (2006) 155–239.

[15] S. Muceli, R. Merletti, Tutorial. frequency analysis of the surface EMG signal: Best practices, J. Electromyogr. Kinesiol. 79 (2024) 102937.

[16] D. Farina, R. Merletti, Comparison of algorithms for estimation of EMG variables during voluntary isometric contractions, Journal of Electromyography and Kinesiology 10 (5) (2000) 337–349.

[17] A. Holobar, D. Zazula, Multichannel blind source separation using convolution kernel compensation, IEEE Trans. on Sig. Proc. 55 (9) (2007) 4487–4496.

[18] A. J. Fuglevand, D. A. Winter, A. E. Patla, Models of recruitment and rate coding organization in motor-unit pools, Journal of Neurophysiology 70 (6) (1993) 2470–2488.